Title
Quantum Mechanics/Molecular Mechanics Modeling of Fatty Acid Amide Hydrolase Reactivation Distinguishes Substrate from Irreversible Covalent Inhibitors

Journal
Journal of Medicinal Chemistry, 56(6)

ISSN
0022-2623

Authors
Lodola, Alessio
Capoferri, Luigi
Rivara, Silvia
et al.

Publication Date
2013-03-28

DOI
10.1021/jm301867x

Published in final edited form as:
J Med Chem. 2013 March 28; 56(6): 2500–2512. doi:10.1021/jm301867x.

Quantum mechanics/molecular mechanics modeling of fatty acid amide hydrolase reactivation distinguishes substrate from irreversible covalent inhibitors

Alessio Lodola[1], **Luigi Capoferri**[1], **Silvia Rivara**[1], **Giorgio Tarzia**[2], **Daniele Piomelli**[3,4], **Adrian Mulholland**[*,5], and **Marco Mor**[*,1]

[1]Dipartimento di Farmacia, Università degli Studi di Parma, I-43124 Parma, Italy

[2]Dipartimento di Scienze Biomolecolari, Università degli Studi di Urbino "Carlo Bo", I-61029, Urbino, Italy

[3]Department of Drug Discovery and Development, Istituto Italiano di Tecnologia, I-16163 Genova, Italy

[4]Department of Anatomy and Neurobiology, University of California, Irvine 92697, USA

[5]School of Chemistry, University of Bristol, Bristol BS8 1TS, UK

Abstract

Carbamate and urea derivatives are important classes of fatty acid amide hydrolase (FAAH) inhibitors that carbamoylate the active-site nucleophile Ser241. In the present work, the reactivation mechanism of carbamoylated FAAH is investigated by means of a quantum mechanics/molecular mechanics (QM/MM) approach. The potential energy surfaces for decarbamoylation of FAAH covalent adducts, deriving from the *O*-aryl carbamate URB597 and from the *N*-piperazinylurea JNJ1661610, were calculated and compared to that for deacylation of FAAH acylated by the substrate oleamide. Calculations show that a carbamic group bound to Ser241 prevents efficient stabilization of transition states of hydrolysis, leading to large increments in the activation barrier. Moreover, the energy barrier for the piperazine carboxylate was significantly lower than that for the ciclohexyl carbamate derived from URB597. This is consistent with experimental data showing slowly reversible FAAH inhibition for the *N*-piperazinylurea inhibitor and irreversible inhibition for URB597.

INTRODUCTION

Fatty acid amide hydrolase (FAAH) is a member of the amidase signature (AS) family of enzymes and it terminates the signal carried by the endocannabinoid arachidonoylethanolamide (AEA), catalyzing its hydrolysis to arachidonic acid and ethanolamine.[1] FAAH has a relatively wide substrate selectivity, as it also catalyzes the hydrolysis of other fatty acid ethanolamides (FAE)s including oleoylethanolamide (OEA) and palmitoylethanolamide (PEA), which are agonists of the peroxisome proliferator-

[*]**Corresponding Author** Marco Mor Phone: +39 0521 905059 Fax: +39 0521 905006 marco.mor@unipr.it Adrian Mulholland Phone: +44-(0)117-928-9097 Fax: +44-(0)117-925-0612 adrian.mulholland@bristol.ac.uk.

Supporting Information SCC-DFTB/CHARMM27 PESs of deacylation of adduct **1a** with a large QM region. Superposition of covalent adduct **1a** on covalent adduct **2a** and of covalent adduct **1a** on covalent adduct **3a**. B3LYP/6-31+G(d)//SCC-DFTB/CHARMM27 PESs for deacylation of covalent adduct **1a** and for decarbamoylation of covalent adducts **2a** and **3a**. Representation of quantum regions of covalent adducts **1a-3a**. H-bond network formed by water molecule W1 in the three considered systems. This material is available free of charge via the Internet at http://pubs.acs.org.

activated receptor (PPAR) subtype alpha.[2] Multiple studies have shown that inactivation of FAAH by active-site directed inhibitors significantly increases the level of FAEs *in vivo,* leading to analgesic, anti-anxiety and anti-inflammatory effects,[3] without producing the unwanted side effects observed with direct CB_1 agonists, including hypothermia, cognitive and motor dysfunctions.[4] FAAH inhibition therefore represents an attractive therapeutic strategy for the treatment of several central nervous system disorders.[5]

FAAH is characterized by a unique Ser-Ser-Lys catalytic triad that is responsible for its ability to cleave amides and esters at similar rates.[6] The catalytic mechanism of FAAH has been widely investigated applying both experimental[7] and computational methods.[8] These investigations, mainly performed using (Z)-9-octadecenamide (oleamide, **1**, Figure 1) as the substrate, have shown that the catalytic process is initiated by the activation of the nucleophile Ser241 by a cooperative action of Ser217 and Lys142. Then, the alcoholate anion of Ser241 attacks the carbonyl group of the substrate, leading to the formation of a tetrahedral intermediate (TI). The reaction proceeds through the protonation of the leaving group which leads to the formation of an acyl-enzyme intermediate.[7,8] The hydrolysis of acylated Ser241 (deacylation) is a necessary event to restore the catalytic state of Ser241 (i.e. with a free hydroxyl group).

Crystal structures of FAAH carbamoylated by different inhibitors allowed the identification of a water molecule possibly responsible for the hydrolysis of the acylated Ser241, thus called the “deacylating water molecule”.[9] This water molecule (W1, Figure 2) occupies a conserved position in different crystal structures, is involved in a complex hydrogen-bond network comprising the catalytic triad, and is well positioned to bring a nucleophilic attack to the covalently functionalized Ser241.[9] The mechanism proposed for FAAH deacylation is based on the cooperative deprotonation by Lys142 and Ser217 of the nucleophile W1 which in turn attacks the carbonyl carbon of the Ser241 acylating portion, generating a TI (Figure 2A, step *i*). This intermediate is expected to collapse rapidly, facilitated by the protonation of Ser241. This reaction leads to the expulsion of Ser241 hydroxyl group and restores a functional enzyme (Figure 2A, step *ii*).

In recent years, the search for selective and potent inhibitors of FAAH has been the subject of intense medicinal chemistry efforts which have lead to the discovery of various chemical classes as shown by the recent literature.[10] Many promising FAAH inhibitors are covalent modifiers of the enzyme, such as *O*-aryl carbamates and piperidinyl-(piperazinyl) aryl ureas.[10] *O*-aryl carbamates, including the reference compound cyclohexylcarbamic acid 3′-carbamoylbiphenyl-3-yl ester (URB597, **2**, Figure 1)[11,12] inhibit FAAH through carbamoylation of Ser241,[13] following a mechanism where Lys142 works as a base and as an acid in distinct steps of the catalytic process.[14,15] X-ray crystallography and mass spectrometry experiments have shown that also cyclic ureas, including the piperidinyl derivative PF-750[16] and the piperazinyl derivative *N*-phenyl-4-(3-phenyl-1,2,4-thiadiazol-5-yl)-1-piperazine-carboxamide (JNJ1661010, **3**, Figure 1),[17] inhibit FAAH through carbamoylation of Ser241. Indeed, the aniline moiety of these compounds serves as a leaving group during catalysis, with the piperidine- or piperazine-1-carboxylic acid fragment forming a tertiary carbamate with Ser241.[18]

Generally, carbamoylating compounds block the catalytic activity of serine hydrolases by trapping the nucleophile residue of the enzyme within an acylenzyme-like intermediate (a carbamoyl serine structure) that is resistant to further hydrolysis (Figure 2B). In other words, the structure of the modified enzyme is such that regeneration of the enzyme, by its further reaction with nucleophiles, becomes a rather slow process, leading to effective inhibition.[19] This is the case for URB597 and *N*-piperazinylurea **3** which react with FAAH generating stable carbamoylated adducts, that are resistant (URB597) or partially resistant (**3**) to

hydrolysis.[20] A recent investigation by Maccarone *et al*,[21] pointed out that stabilization of the carbamoyl serine might not be the only determinant for long-lasting inactivation of FAAH. Indeed, while carbamates having a 3′-carbamoylbiphenyl-3-ol leaving group (i.e. URB597) acted as irreversible inhibitors of mouse FAAH, the corresponding carbamates having a 3-(3-carbamoyl-pyrrol-1-yl)phenol leaving group acted as reversible inhibitors, giving recovery of enzymatic activity after 18-hrs dialysis. This finding suggests that the leaving group portion of carbamoylating agents may also influence the kinetics of FAAH reactivation.

In this context, atomistic investigations aimed at the elucidation of the precise mechanism by which carbamoylating agents achieve the (pseudo)-irreversible inhibition of FAAH are critical to identify their chemical determinants. Understanding the inhibitory mechanism at the atomic level should help in determining the crucial difference(s) between substrates and inhibitors, potentially helping the design of the next generation of FAAH covalent inhibitors.

In the present paper, starting from adduct **1a** (Figure 1) we investigated the process of FAAH deacylation challenging the hydrolytic mechanism proposed by Mileni *et al* (Figure 2A),[9] by applying a quantum mechanics/molecular mechanics (QM/MM) approach.[22] This approach is widely used for the investigation of biomolecular processes,[23] including reactions catalyzed by pharmaceutically relevant enzymes.[24] We next investigated the process of FAAH decarbamoylation starting from two distinct FAAH carbamoylated adducts. The first adduct involved URB597, which gave a secondary carbamate at Ser241 (adduct **2a**, Figure 1), while the second involved the *N*-piperazinylurea **3**, which in turn gave a tertiary carbamate at Ser241 (adduct **3a**, Figure 1). Finally, the identified minimum energy paths of FAAH decarbamoylation were compared to that obtained for FAAH deacylation, to gather insights into the fine mechanism of FAAH inhibition. Potential energy barriers, structural rearrangement, and the stabilizing contribution provided by the protein environment were thoroughly analyzed.

RESULTS AND DISCUSSION

Reaction path calculations

The deacylation and decarbamoylation reactions were modeled in two main steps, starting from the FAAH-acylated adduct **1a** (including a octadec-9-enyl fragment from oleamide) or from FAAH-carbamoylated adducts **2a** and **3a**, including carbamoylating fragments of URB597 and compound **3**. According to the mechanism depicted in Figure 3, these steps were: (*i*) attack of a conserved water molecule (W1) and formation of a TI; (*ii*) protonation of the leaving group, followed by its subsequent expulsion with formation of free Ser241. For these crucial steps, potential energy surfaces (PESs) were investigated using the adiabatic mapping approach applying a hybrid QM/MM potential. Specifically, the self-consistent charge-density functional tight binding (SCC-DFTB) method [25] was used in combination with CHARMM27 force field,[26] (see Experimental Section for details) to calculate the energy of the system along the defined reaction coordinates (see below).

Step (*i*) consisted of several events: a proton was initially abstracted from the water molecule W1 and transferred to the neutral Lys142, *via* the bridging residue Ser217 (events ***x*** and ***y***, Figure 3). Then, the activated water W1 attacked the carbonyl carbon of the acyl or carbamoyl group (event **z**), leading to the formation of the TI. For this purpose, step (*i*) was modeled by restraining the following two reaction coordinates (Figure 3): R_X, defined as $[d(O_w, H_w) - d(O_2, H_w) - d(O_w, C)]$, describing proton abstraction from water W1 by Ser217 and nucleophile attack by W1; and R_Y, defined as $[d(O_2, H_2)] - d[(N, H_2)]$, which described the proton transfer between Ser217 and Lys142.

Also step *ii* was a complex process, as it involved the breakage of the bond between the hydroxyl oxygen of Ser241 and the carbonyl carbon of the acyl or carbamoyl fragments (event ***r***), assisted by a double proton transfer involving Ser217 (event ***s***) and Lys142 (event ***t***). Step (*ii*) was thus modeled using reaction coordinate R_S, defined as [d(O_1, H_W) − d(O_2, H_W) + d(O_2,C)], describing protonation and expulsion of Ser241, and R_T defined as [d(N, H_2]−d(O_1,H_2)] which accounted for the movement of proton H_2 from Lys142 to Ser217.

Deacylation of adduct 1a

The SCC-DFTB/CHARMM27 PESs of FAAH deacylation are reported in Figure 4. The potential energy surfaces have a smooth shape, indicating that the employed reaction coordinates and modeling procedure are able to describe the essential details of the reaction. The PES relative to step *i* (formation of the TI) is reported in the left panel. The change in energy during the nucleophilic attack of water molecule W1 (event ***z***), assisted by deprotonation of Ser217 (event ***y***), can be followed along Rx, while the change in potential energy during the protonation of Lys142 (event ***x***) can be observed along Ry. The minimum energy path (MEP) for step *i* indicated the presence of a concerted mechanism. Indeed, the MEP connecting the acylenzyme (**A**) with the TI (**C**) goes approximately through the middle of the surface. The highest point along the MEP, corresponding to the transition state (TS1, **B**), has an energy of 16.6 kcal mol^{-1} compared to the acylenzyme (**A**). Visual inspection of **B** shows that the proton abstraction from the water molecule to Ser217 is nearly complete in this configuration. The distance of the moving proton H_w from the oxygen of Ser217 (H_w–O_2) is 1.11 Å (1.02 Å at the TI), while the distance to the water oxygen O_w is 1.38 Å (Table 1). In the TS1, the proton transfer involving Ser217 and Lys142 is already complete, the H_2–N distance being the same as that of the TI (1.06 Å).

The distance of the W1 oxygen (O_W) to the carbonyl carbon decreases from 2.48 Å in the acylenzyme to 1.84 Å of the TS1, indicating that the nucleophilic attack is occurring. The C–O_w distance shortens constantly from the TS1 to the TI, where it reaches its equilibrium distance of 1.47 Å (Table 1).

The TI (**C**) is less stable than the acylenzyme adduct by 12.5 kcal mol^{-1}, indicating its transient character. On the other hand, this configuration is stabilized by the FAAH oxyanion hole, which forms a network of hydrogen bonds with the negatively charged oxygen of the substrate (Figure 4), as also reported in previous calculations.[8] Interestingly, an accessory water molecule (W2)[9] is found to interact with the carbonyl oxygen of the acyl portion of **1** in both the TS1 and TI (Figure 4, bottom panel), assisting the stabilization of the incoming negative charge on the oxygen atom.

The SCC-DFTB/CHARMM27 PES associated with step *ii* of the reaction (TI collapse) is reported in Figure 4. The change in energy during the expulsion of Ser241 side chain from the TI (***r***), assisted by protonation performed by Ser217 (***s***), can be followed along R_S. The change in energy during the H_2 proton transfer from Lys142 to Ser217 (***t***) can be observed along R_T. The PES of step *ii* shows a MEP that connects the TI (**C**) with the products of the reaction (the free enzyme and oleic acid, **E**), moving approximately across the middle of the surface. No stable species are found during this reaction step, suggesting that the protonation events (***s*** and ***t***) are tightly coupled with leaving group expulsion (***r***).

However, visual inspection of the TS2 structure (**D**), shows that protonation of Ser241 O_1 by Ser217 (H_w–O_1 distance 1.29 Å) is occurring during the breakage of the O_1-C bond (O_1-C distance 1.91 Å). On the contrary, the transfer of H_2 from Lys142 back to Ser217 only begins at this point of the reaction (N–H_2 distance 1.11 Å). The energy of the TS2 (**D**) is 14.3 kcal mol^{-1} (relative to the acylenzyme **A**), ~2 kcal mol^{-1} lower than that calculated for the formation of the TI. This suggests that step *i*, rather than step *ii*, is the rate-liming event

for FAAH deacylation. However, the TI occupies a flat area of the PES suggesting that formation and collapse of TI are tightly coupled events. Finally, the product of the reaction **E** is less stable than the acylenzyme by 8.2 kcal mol^{-1}.

QM/MM modeling of FAAH deacylation was repeated employing an extended QM region which included residues belonging to the oxyanion hole of FAAH, such as Ile238, Gly239 and Gly240.

The resulting SCC-DFTB/CHARMM27 PESs (Figure S1) are comparable to those reported in Figure 4, indicating that the oxyanion hole can be treated at MM level without significantly affecting the reaction energetics (Table S1).

Decarbamoylation of adduct 2a

The SCC-DFTB/CHARMM27 PESs for FAAH decarbamoylation starting from covalent adduct **2a** are reported in Figure 5. The surface relative to step *i* is reported in the left panel. The change in energy during W1 deprotonation by Ser217 (***y***) and the subsequent nucleophilic attack on the carbamoylated Ser241 (***z***) can be followed along Rx, while the change in energy during the Ser217-Lys142 proton transfer (***x***) can be observed along R_Y. As seen for deacylation, the minimum energy path (MEP) connecting the carbamoylenzyme (**A**) to the TI (**C**) goes diagonally on the PES surface, indicating that reaction processes ***x***, ***y*** and ***z*** are concerted. The SCC-DFTB/CHARMM27 energy barrier for the first step of FAAH decarbamoylation is 28.3 kcal mol^{-1}, ~ 12 kcal mol^{-1} higher than the barrier found for the first step of FAAH deacylation.

Analysis of TS1 (**B**) shows that the proton H_w is nearly completely transferred to the accepting oxygen (O_2) of Ser217 (O_2-H_w distance = 1.09 Å, Table 2) in this configuration, while the removal of H_w from the W1 oxygen (O_w-H_w distance = 1.44 Å) is not yet complete. Proton H_2 is almost bound to the side-chain nitrogen atom (N) of Lys142 (N-H_2 distance = 1.06 Å), at this stage of the reaction. The distance between the W1 oxygen (O_w) and the carbonyl carbon of the carbamoyl portion of URB597 is considerably decreased from the 2.66 Å at configuration **A** to 1.82 Å at TS1. Furthermore, the finding that carbamate group significantly deviates from planarity confirms that the nucleophilic attack is occurring. Visual inspection of the TI structure (**C**) confirms the presence of a new bond between the water molecule W1 and the carbonyl carbon of the inhibitor (O_w–C distance = 1.57 Å). Conversely, the O_2-H_w and N-H_2 distances underwent only minor adjustments (Table 2), indicating that the geometry of the TI closely resembles that of TS1, consistent with their proximity to one another on the PES. As a consequence, the TI has a very high energy, only 1 kcal mol^{-1} lower than the energy of TS1.

The PES for step *ii* is shown in the right panel of Figure 5. The change in potential energy during protonation of the leaving group (event ***s***) and its expulsion (event ***r***) is described by reaction coordinate R_S, while the change in the energy during deprotonation of Lys142 (event ***t***) can be observed along R_T. Analysis of the TS2 (**D**) shows that, at this stage of the reaction, the events ***s*** and ***r*** are almost complete, as indicated by O_2-H_W, O_1–H_W, and C-O_1 distances of 1.07 Å, 1.50 Å and 1.79 Å, respectively. In contrast, the proton transfer from Lys142 to Ser217 has not occurred yet, as the H_2 was still bound to Lys142 (O_2-H_2 = 1.70 Å; N-H_2 = 1.07 Å). The energy of **D** is 28.9 kcal mol^{-1}, only ~1 kcal mol^{-1} higher than TI, confirming that step *i* and *ii* are tightly coupled, similar to what was observed for FAAH deacylation. The final proton transfer (***t***) is spontaneous, as no barrier is found between **D** and **E** on the PES. Configuration **E**, is ~9 kcal mol^{-1} less stable than the carbamoylenzyme **A**.

Decarbamoylation of adduct 3a

The SCC-DFTB/CHARMM27 PESs for FAAH decarbamoylation starting from covalent adduct **3a** are reported in Figure 6. The surface relative to step *i* is shown in the left panel. The change in energy during W1 deprotonation and subsequent nucleophilic attack can be followed along R_X, while the change in the potential energy during the protonation of Lys142 can be observed along R_Y. Similarly to what was observed for decarbamoylation of **2a**, the MEP connecting **A** to the TI (**C**) shows a concerted reaction. At TS1 (**B**), proton H_2 is still bound to Lys142 (O_2-H_2 = 1.74 Å; N-H_2 = 1.06 Å), while the proton abstraction of H_w (from W1) by Ser217 is almost complete, with O_2-H_W distance of 1.10 Å, similar to 1.00 Å distance at the TI. TS1 shows an incoming nucleophilic attack, the O_W-C distance being only 1.83 Å, similar to the final value of 1.53 Å at the TI. The energy content of the TS1 (**B**) is 21.9 kcal mol^{-1} relative to the carbamoylenzyme **A**. The TI (**C**) has an energy only a few kcal mol^{-1} lower than the TS1 (19.6 kcal mol^{-1} compared to **A**), as also observed in the case of decarbamoylation of FAAH from covalent adduct **2a**.

The reaction energetics of step *ii* are reported on the PES in the right panel of Figure 6. Protonation (event ***s***) and expulsion (event ***r***) of the Ser241 leaving group are described by the reaction coordinate R_S, while the Lys142-Ser217 proton transfer (event ***t***) is described by R_T. The MEP links the TI (**C**) with the product of the reaction (**E**), moving approximately across the middle of the surface. No stable species are found during this reaction, suggesting that the two protonation events (***s*** and ***t***) are tightly coupled with the expulsion of the leaving group (***r***). Analysis of TS2 (**D**) shows that the expulsion of leaving group Ser241 is advanced (O_1-C = 2.12 Å, Table 3) in this configuration. This process is assisted by a double proton transfer (involving Ser217 and Lys142, Figure 2) as shown by the O_1-H_W and N–H_2 distances of 1.04 Å and 1.18 Å, respectively, at the TS2 (Table 3). The potential energy barrier required to overcome TS2 (**D)** is 23 kcal mol^{-1} (relative to **A**), ~3 kcal mol^{-1} higher than the barrier found for step *i*. Finally, the product of the reaction **E** (composed by the free enzyme and 4-(3-phenyl-1,2,4-thiadiazol-5-yl)piperazin-1-yl carbamic acid) is calculated to be less stable than the carbamoylenzyme **A** by 15.8 kcal mol^{-1}.

Overall deacylation and decarbamoylation reaction profiles

Figure 7 summarizes the SCC-DFTB/CHARMM27 potential energy profiles for FAAH deacylation in the presence of the acylating portion of oleamide and for FAAH decarbamoylation in the presence of the carbamoylationg portions of URB597 or *N*-piperazinylurea **3**. The calculated energies indicate that, for FAAH deacylation, formation of TI (rather than its collapse) represents the rate-limiting step of the process. Conversely, the energy profile for FAAH decarbamoylation indicates that this process depends on both TI formation and collapse, with no single step being clearly rate-limiting. Decarbamoylation of FAAH adducts needs to overcome a significantly higher energy barrier than deacylation, consistent with the roles of covalent inhibitors and a substrate, respectively.

The energy barrier of 28.6 kcal mol^{-1} for decarbamoylation of **2a**, (the adduct formed by FAAH with URB597) was higher than that (22.9 kcal mol^{-1}) calculated for **3a** (the adduct formed by FAAH and **3**). These values are consistent with the result of dialysis experiments on both rat[17] and human[20] FAAH, where URB597 behaved as an irreversible inhibitor, while inhibition by *N*-piperazinylurea **3** was slowly reversible.

QM/MM calculations based on the adiabatic mapping approach can be considerably affected by the starting geometry of the reactant complex.[27] SCC-DFTB/CHARMM27 calculations were therefore performed for alternative conformations of FAAH covalent adducts. For each system, seven additional FAAH structures were extracted from a QM/MM-MD trajectory (see Experimental Section) and employed as starting geometries to build PESs for

deacylation or decarbamoylation reactions. The PES shapes were not significantly influenced by the starting geometry of the reactants, although moderate differences were observed in the calculated potential energies. The results of these additional simulations are summarized in Table 4, where the SCC-DFTB/CHARMM27 energy of the stationary points are expressed as mean value ± standard error of the mean (SEM). The averaged energy values are consistent with those reported in Figure 7, confirming that *i)* Ser241 deacylation is energetically favored over decarbamoylation, *ii)* the barrier for Ser241 decarbamoylation of the irreversible inhibitor URB597 is higher than that obtained for the slowly-reversible inhibitor **3**.

Comparison with single-point calculations in gas phase: the effect of catalytic site on TI stabilization

To examine the stabilization provided by FAAH during the simulated reactions, single-point energy calculations on the isolated QM regions were carried out starting from geometries corresponding to the grid points of the PESs reported in Figures 4, 5 and 6. The resulting gas-phase SCC-DTFB energies for geometries corresponding to the stationary points of QM/MM PESs are reported in Figure 8. The three profiles have similar shapes and, as expected, show significantly higher energy values for the TSs, compared to those calculated in the presence of FAAH. More importantly, in the absence of the enzyme the TIs are not minimum-energy structures on the PESs, but the points with highest energy. While for deacylation of adduct **1a** the TI has an energy 83.8 kcal mol^{-1}, compared to the reactants, in the case of decarbamoylation the difference is 91.3 kcal mol^{-1} for adduct **2a** and 86.1 kcal $mol^{-1}$for adduct **3a**. This indicates that the carbamoylated serine is less prone to react with the water molecule W1 than the acylated one, reflecting the higher solvolytic stability of carbamic acid *O*-alkyl esters (as in the case of adducts **2a** and **3a**) over carboxylic acid *O*-alkyl ester (as for adduct **1a**).

Enzymes usually posses a specific environment which complements the changes in the electronic structure of the “substrate” during the catalyzed reactions.[22,23] This provides an effective way of reducing the activation energy of chemical transformations. The environmental effect provided by FAAH during the reaction of deacylation/decarbamoylation can be estimated by subtracting the SCC-DFTB energy of the isolated QM region from the total SCC-DTFB/CHARMM27 energy.

As previously reported for simulations of FAAH acylation,[8] the active site provides increasing stabilization of the reacting system as the deacylation or decarbamoylation proceeds until the TI is reached. It is evident that FAAH stabilizes the TS structures (**B** and **D**), but it stabilizes the TIs (**C**) even more (Figure 9), due to its oxyanion hole.[8]

Figure 9 shows that the stabilization of the TI provided by FAAH for decarbamoylation of covalent adducts **2a** and **3a** (−63.5 and −66.5 kcal mol^{-1}, respectively) is significantly smaller than that calculated for deacylation of covalent adduct **1a** (−71.3 kcal mol^{-1}). In other words, the replacement of the acylating portion of adduct **1a** with the carbamoylating ones of adducts **2a** and **3a** leads to a suboptimal stabilization of the tetrahedral intermediate. This lack of TI stabilization increases the barrier height for completing the decarbamoylation processes, eventually leading to enzyme inhibition.

Decomposition Analysis

The contribution of individual residues to the stabilization of the TI was analyzed by decomposition analysis (see Experimental Section), selecting configuration **A** (i.e. adduct **1a**, **2a** or **3a** depending on the considered reaction) as the reference structure. The effects of each amino acid or water molecule on TI stabilization are reported in Figure 10.

Decomposition analysis was performed for all eight starting conformations of covalent adducts **1a**, **2a** and **3a**. The results of these calculations reported here (Figure 10) are referred to a representative conformation for each system (see Experimental Section).

For deacylation of adduct **1a**, the main contribution to lowering the potential energy of the TI is from the auxiliary water W2. This water molecule is a structurally conserved element of the FAAH active site[9] and it was found here to form a short hydrogen bond (H-bond) with the carbonyl oxygen of the acyl group at Ser241 (Table S2). Among the residues forming the oxyanion hole of FAAH (i.e. Ile238, Gly239, Gly240 and Ser241), Ile238 and Ser241 are the most important in stabilizing the TI, due to their backbone-NH groups which form H-bonds with the carbonyl oxygen of the acyl group at Ser241. Other important residues are Thr236, Ser218 and Arg243. The first two residues contribute to TI stabilization by accepting hydrogen-bonds from Lys142. Arg243 interacts with the oxyanion hole, helping the stabilization of the negatively charged oxygen of the acyl group bound to Ser241.

Similar stabilizing effects on the TI are observed for decarbamoylation of covalent adduct **2a** (involving URB597) with the exception of the role played by water W2. Visual inspection of the TI geometry shows that W2 does not form a H-bond with the oxygen of the carbamoyl group at Ser241, as evidenced by the interatomic distances reported in Table S2. The lack of this interaction is due to the peculiar accommodation of the carbamic moiety of URB597 at the FAAH active site (compared to that of acyl chain of oleamide), which is driven by a H-bond between the carbamic NH group and the backbone oxygen of Ser193 (Figure S2).

In the case of covalent adduct **3a** (involving *N*-piperazinylurea **3**), the individual effects of FAAH active site residues on the decarbamoylation are qualitatively similar to those observed for deacylation of **1**, including W2. The tertiary carbamoylating portion of *N*-piperazinylurea **3** is accommodated at the FAAH active site with a binding conformation similar to that of the acylating portion of oleamide (Figure S3). This allows the auxiliary water molecule W2 to form a H-bond with the carbonyl oxygen of the carbamate group at the TI (Table S2), significantly stabilizing this configuration.

High-level corrections

To improve the accuracy of the reaction energetics for both deacylation of covalent adduct **1a** and decarbamoylation of covalent adducts **2a** and **3a**, the potential energy surfaces obtained at SCC-DFTB/CHARMM27 level were corrected by means of B3LYP calculations (see Experimental Section). The resulting B3LYP/6-31+G(d)//SCC-DFTB/CHARMM27 PESs (Figure S4) relative to deacylation of adduct **1a** (involving oleamide) are to some extent similar to those calculated at SCC-DFTB/CHARMM27 level (Figure 4). While both methods identified TS1 as the highest point along the path (Table 5), B3LYP calculations indicated that configuration **D** (TS2) is no more a stationary point on the PES of step *ii*. TI formation and collapse appears tightly coupled at this level of theory (Figure S4).

B3LYP/6-31+G(d)//SCC-DFTB/CHARMM27 surfaces for decarbamoylation of covalent adducts **2a** (involving URB597) and **3a** (involving *N*-piperazinylurea **3)** were very similar to the PESs calculated at SCC-DFTB/CHARMM27 level, both in terms of position and energetics of the relevant stationary points **A**-**E** (Figures S5 and S6).

Altogether B3LYP/6-31+G(d)//SCC-DFTB/CHARMM27 calculations (Table 5) confirm the analysis performed at lower level indicating that Ser241 deacylation is energetically favored over Ser241 decarbamoylation, and that energy barrier for Ser241 decarbamoylation of adduct **2a** is significantly higher than that for adduct **3a.**

CONCLUSIONS

The most important time-dependent inhibitors of FAAH belong to the *O*-aryl carbamate or piperidinyl/piperazinyl-aryl urea classes, here exemplified by URB597 and *N*-piperazinylurea **3**. These compounds have been shown by crystallography to react with Ser241 to form a carbamoylated intermediate. The carbamoylated form of FAAH is significantly more resistant to hydrolysis than the corresponding acylated form (produced by the reaction of the enzyme with a substrate) and thus is expected to be responsible for time-dependent and persistent inhibition of FAAH activity. To gain insights into the mechanism of FAAH inhibition by carbamoylating agents, we first investigated the mechanism of deacylation for the acylated form of FAAH, starting from the FAAH-oleamide adduct **1a**. Calculations show that a mechanism involving a conserved water molecule (W1) as a nucleophile[9] is energetically realistic, with a calculated barrier (16.6 kcal mol^{-1}) consistent with experimental data.[28] A similar mechanism was then modeled for decarbamoylation of covalent adducts **2a** and **3a**, formed by FAAH with URB597 and *N*-piperazinylurea **3**, respectively. The calculated energy barriers were of 28.6 kcal mol^{-1} and 22.9 kcal mol^{-1} for adducts **2a** and **3a**, respectively, significantly higher than that for deacylation of **1a**. The calculated energy barriers for FAAH decarbamoylation are also in qualitative agreement with dialysis data, showing that, under the same experimental conditions: *i)* human and rat FAAH do not recover any catalytic activity after inhibition by URB597, whilst *ii)* human and rat FAAH partially recover catalytic activity after inhibition by *N*-piperazinylurea **3**.[17,20]

While a recent paper by Maccarone *et al.*[21] pointed out that reactivation of carbamoylated FAAH might also be influenced by the leaving group portion of inhibitors, our calculations show that the spatial arrangement of the carbamoylating portion at the active site is crucial for the irreversible nature of FAAH inhibition. In particular, gas-phase calculations and decomposition analysis indicate that the secondary carbamic portion of the FAAH-URB597 adduct remarkably increases the barrier of water-promoted reactivation by reducing the electrostatic stabilization provided by the active site at the main transition states and intermediates of the reaction. Detailed calculations of this type may help to design novel covalent inhibitors with the desired mechanism of action. These results provide a further indication of how QM/MM calculations can contribute to practical questions of drug development.

EXPERIMENTAL SECTION

Application of the QM/MM potential

The CHARMM program (version c30b2)[29] was employed to build FAAH-substrate and FAAH inhibitor systems, as well as to perform energy minimizations and molecular dynamics simulations. The CHARMM27 all-atom force field[26] was used in combination with the self-consistent charge-density functional tight binding (SCC-DFTB) method,[25] as implemented in the QM/MM module of CHARMM.[30] The SCC-DFTB method is an approximate density functional theory (DFT) method and it is more efficient than *ab initio* QM/MM approaches. Despite its high computational efficiency, SCC-DFTB has been shown in many cases to provide geometries and relative energies comparable to DFT and *ab initio* calculations.[25] The SCC-DFTB model has been tested on several enzymes,[31] including FAAH.[32] In particular, the remarkable ability of FAAH in hydrolyzing the amide substrates faster than the ester ones has been found to be satisfactorily reproduced by the SCC-DFTB/CHARMM27 protocol[32] applied here. A relatively large quantum mechanical region of 73 atoms was defined for the FAAH covalent adduct **1a** (Figure S7). This includes the catalytic water W1, the (Z)-octadec-9-enyl fragment of oleamide and parts of the side chains of Lys142, Ser217 and Ser241. In the adduct **2a**, the cyclohexyl carbamic acid

portion of URB597, parts of Lys142, Ser217 and Ser241 side chains and water W1 were included in QM region, for a total of 42 atoms (Figure S8). In the case of the FAAH-covalent adduct **3a**, the 4-(3-phenyl-1,2,4-thiadiazol-5-yl)piperazin-1-yl carbamic acid portion of compound **3**, parts of Lys142, Ser217 and Ser241 side chains, and W1 molecule were included in QM selection, for a total of 53 atoms (Figure S9). In these three systems, the QM region had a neutral total charge and in all of them, three HQ-type 'link atoms'[22b] were introduced to saturate the shells of QM-atoms covalently bonded to MM-atoms.

The QM/MM approach used here includes bonded and non-bonded interactions between the QM and MM systems and accounts for the essential effect of the protein on the modeled reactions. Van der Waals and bonded interactions were described by MM terms, with standard CHARMM27 parameters used for the QM and MM atoms. Electrostatic interactions were treated by calculating the Coulombic interactions between the Mulliken charges of the QM atoms and the MM partial atomic charges.[30] A group-based non-bonded cut-off of 12 Å was applied and atoms further than 16 Å from the Ser241 hydroxyl oxygen were kept fixed. With the exception of these boundary restraints, all the other atoms were free to move during the calculations. In the case of covalent adduct **1a**, a larger QM region was also defined and employed for testing the effect of the QM/MM partition scheme on the reaction energetics, comparing the results with those obtained for the 73 atom QM-region. The extended QM region was composed by water W1, the (Z)-octadec-9-enyl fragment of oleamide, parts of the side chains of Lys142 and Ser217, and backbone and side chains of Asp237, Ile238, Gly249, Gly240 and Ser241, for a total of 125 atoms and a net charge of $-1e$ (Figure S10).

Preparation of the protein-ligand models

The structures of the covalent adducts **1a** and **3a** were prepared starting from the X-ray coordinates of the adduct between the humanized-rat (h/r) variant of FAAH and the inhibitor PF-3845 (PDB code 3LJ6),[9] following procedures similar to those used in previous successful modeling of FAAH.[14,15] The carbamoylating fragment of PF-3845 was transformed into the (Z)-octadec-9-enyl group of oleamide or into the 4-(3-phenyl-1,2,4-thiadiazol-5-yl)piperazin-1-yl group of compound **3**. The coordinates of the adduct **2a** were taken from the X-ray crystal structure of the h/r variant of FAAH-URB597 (PDB entry 3LJ7).[9] Hydrogen atoms were added with the HBUILD routine in CHARMM. Conventional protonation states (physiological pH) were assigned to all the amino acids, except for Lys142 that was modeled in its neutral form. All protein residues and the crystallographic water molecules containing at least one atom within 25 Å of the system centre (defined as the side chain oxygen of Ser241) were included in the models. The three systems were solvated by superimposing a 25 Å radius sphere of pre-equilibrated TIPS3P water molecules (i.e. the CHARMM-type variant of TIP3P water).[33] After solvation, the systems contained 7756 atoms in the case of adduct **1a**, 7610 for adduct **2a** and 7741 for adduct **3a**.

MM-energy minimization with all non-water atoms fixed was then carried out with 500 steps of steepest descent (SD) followed by 2500 steps of Adopted Basis Newton–Raphson (ABNR). Finally, the three systems were fully minimized using ABNR, without any constraint to a gradient tolerance of 0.01 kcal mol^{-1}.

Protein-ligand adducts were prepared for stochastic boundary molecular dynamics (SBMD) simulation.[34] Stochastic boundary conditions were applied by separating the systems into two regions: the reaction region, consisting of all atoms within 21 Å of the system centre, and the buffer region, containing all other atoms outside the 21 Å sphere. While the reaction region was treated with Newtonian dynamics, the buffer region was described by Langevin dynamics. Furthermore, a deformable boundary potential was imposed on the water molecules to prevent their diffusion from the reactive site. In the buffer region, the Langevin

equations of motion impose a friction coefficient and a random force on heavy atoms, which allow the buffer region to act as a heat bath. Friction coefficients of 250 ps^{-1} for non-hydrogen protein atoms and 62 ps^{-1} on water oxygen atoms were used, as applied in previous simulations on FAAH.[8d]

SBMD simulations were performed using the SCC-DFTB/CHARMM27 potential. The systems were heated from 10 to 310 K in three separate and consecutive steps of 50 ps: *i*) from 10 to 100 K, *ii*) from 100 to 200 K, and, *iii*) from 200 to 310 K. Finally, these three systems were simulated for 2 ns at 310 K, in the SBMD regime. The SHAKE algorithm was applied with a time step for integration of 1 fs.

For each system, after 600 ps of simulation, one snapshot every 200 ps of QM/MM SBMD simulation was collected for mechanistic study, giving a total of 8 starting structures. The resulting 24 structures were minimized to a gradient tolerance of 0.01 kcal mol^{-1} $Å^{-1}$ with the QM/MM potential, freezing all heavy atoms further than 16 Å from the reaction center, and then employed to model the deacylation or decarbamoylation reaction. The same equilibration protocol, including the final QM/MM energy minimization, was employed for covalent adduct **1a** with the extended QM region.

Calculation of the Potential Energy Surfaces

Potential energy surfaces (PES) of the deacylation and decarbamoylation reactions were explored at SCC-DFTB/CHARMM27 level of theory, by means of an adiabatic mapping method.[23] Reaction coordinates were defined for reaction steps *i* and *ii* (Figure 3) and restrained sequentially to move the system along the given reaction path. In the case of step *i,* the reaction coordinates were R_X, defined as $[d(O_w, H_w) - d(O_2, H_w) - d(O_w, C)]$, describing proton abstraction from water W1 by Ser217 and nucleophile attack by W1; and R_Y, defined as $[d(O_2, H_2)] - d[(N, H_2)]$, which described the proton transfer between Ser217 and Lys142. For step *ii* (Figure 3) the reaction coordinates were R_S, defined as $[d(O_1, H_W) - d(O_2, H_W) + d(O_2,C)]$, describing protonation and expulsion of Ser241, and R_T defined as $[d(N, H_2]-d(O_1,H_2)]$ which accounted for the movement of proton H_2 from Lys142 to Ser217.

Reaction coordinate restraints were applied by means of the RESD command implemented in the CHARMM program. A force constant of k=5000 kcal mol^{-1} $Å^{-2}$ was used to restrain all the defined coordinates. The values for the restrained distances were increased in steps of 0.1 Å to force the system across the barrier for a specific reaction step. ABNR energy minimizations of all the generated structures were performed to a gradient tolerance of 0.01 kcal mol^{-1} $Å^{-1}$ using a SCC-DTFB/CHARMM27 potential. The final energy of a structure (as indicated on the potential energy surfaces) was obtained by performing single-point energy calculations at SCC-DFTB/CHARMM27 level, excluding the energy contribution from the applied restraint. Furthermore, the structures of energy minima were determined more accurately by performing additional geometry optimizations with no restraints on the reaction coordinates. The PESs explored here allow the determination of basic mechanistic features of a given reaction, such as the identification of approximate transition states and intermediates. However, they do not account for zero-point energy, nor for the influence of hydrogen tunneling effects that are expected to lower the calculated barriers by few kcal mol^{-1}, nor do they include entropy, which would conversely make free energy barriers typically somewhat larger than potential energy barriers.[23] As shown in previous work, potential energy surfaces alone can provide useful insight into important features in FAAH. It is important, however, to consider the effects of conformational variability, as we do here by investigating multiple structures from MD simulations.

The detailed description of the reaction energetics reported for covalent adducts **1a**, **2a**, and **3a** in the Results and Discussion section is based on the snapshot (i.e. starting conformation of the reactants) giving the lowest SCC-DFTB/CHARMM27 energy barriers. For covalent adducts **1a** and **2a**, the best snapshot was the one collected after 1200 ps of SBMD simulation, while for adduct **3a**, the snapshot giving the lowest barrier was the one collected after 600 ps. These snapshots were also used as reference structures for single-point calculations *in vacuo* and for active site decomposition analysis.

For adduct **1a** with the extended QM region, a single snapshot (collected after 1000 ps of SBMD simulations) was employed for QM/MM reaction modeling of the deacylation process.

High-level corrections

SCC-DFTB/CHARMM27 potential energy surfaces were corrected at B3LYP/6-31+G(d) level using a previously developed approach,[35,36] that has been also applied to FAAH.[8a,14,15] Briefly, the geometries of the QM-atoms of every structure of each SCC-DFTB/CHARMM27 surface were isolated, and gas-phase energy calculations were performed at the SCC-DFTB and B3LYP/6-31+G(d) levels, respectively. Thus, for the results presented here, approximately 1800 B3LYP calculations were needed (i.e., around 600 for each covalent adduct).[37] The corrected energies were obtained by subtracting from the total QM/MM energy the SCC-DFTB energy of the isolated QM region and adding the B3LYP energy. The B3LYP corrected potential energy surfaces consist therefore of the B3LYP vacuum energy, of the CHARMM27 MM energy, and of the SCC-DFTB/CHARMM27 QM/MM interaction energy.

Single-point calculations *in vacuo* and enzyme stabilization energy

To quantify the relative stabilization provided by FAAH at important points during the reaction, the SCC-DFTB energy of the QM region alone (E_{QM}*vacuo*), at the corresponding QM/MM optimized geometry, was re-calculated for each stationary point identified along the deacylation or decarbamoylation of FAAH covalent adducts **1a**-**3a**.

We then defined the stabilization energy of the MM part of the enzyme on the QM part as:

$$E_{stabilization}=E_{total} - E_{QM\mathit{vacuo}}$$

where the total energy of each system has the form of a potential energy and it is defined as:

$$E_{total}=E_{QM/MM}+E_{MM}$$

The EQM/MM includes the self-consistent energy of the QM atoms and the interaction energy between the QM and MM regions, including electrostatic and polarization effects as well as an MM term which includes van der Waals interactions between QM and MM atoms. E_{MM} is the classical contribution of the energy arising from MM part. Thus, the stabilization energy is the amount by which a QM region structure is stabilized by the environment relative to the reactant, and it has been shown to provide insight into a number of enzyme-catalyzed reactions.[38]

Active site decomposition analysis

To obtain qualitative information about the contribution of specific residues to the total QM/MM energy difference between the reactants (state **A** in Figures 4, 5, 6) and the

corresponding tetrahedral intermediates (state **C**), energy decomposition analyses were performed with a procedure similar to those used previously.[39] Geometries corresponding to states **A** and **C** were taken from deacylation and decarbamoylation pathways and used as follows: *i)* FAAH active site residues (included in the MM part and within 6 Å of Ser241 oxygen atoms) were removed from each system once at a time; *ii)* after every deletion, the total energy of the system was recalculated by single point calculation at SCC-DFTB/CHARMM27 level; *iii)* the contribution of residue *i* to the stabilization of tetrahedral intermediate (state **C**), with respect to the reactants (state **A**) was calculated as:

$$\left(E_{total,C} - E_{total,Ci}\right) - \left(E_{totalA}, -E_{total,Ai}\right)$$

where $E_{total,C}$ was the energy of state **C** and $E_{total,Ci}$ the energy of state **C** after deletion of residue *i* from the active site. Similarly, $E_{total,A}$ was the energy of state **A** and $E_{total,Ai}$ the energy of state **A** after deletion of residue *i* from the active site.

Supplementary Material

Refer to Web version on PubMed Central for supplementary material.

Acknowledgments

This work was supported by MIUR (Ministero dell'Istruzione, dell'Università e della Ricerca) and University of Parma. A.J.M. is an EPSRC Leadership Fellow. Mauro Mileni is acknowledged for useful discussions.

ABBREVIATIONS USED

FAAH	fatty acid amide hydrolase
FAE	fatty acid ethanolamide
MEP	minimum energy path
OEA	oleoylethanolamide
PEA	palmitoylethanolamide
PES	potential energy surface
PPAR	peroxisome proliferator-activated receptor
QM/MM	quantum mechanics/molecular mechanics
SBMD	stochastic boundary molecular dynamics
SCC-DFTB	self-consistent charge-density functional tight binding
TI	tetrahedral intermediate
TS	transition state

REFERENCES

1. Piomelli D. The molecular logic of endocannabinoid signaling. Nat. Rev. Neurosci. 2003; 4:873–884. [PubMed: 14595399]
2. Labar G, Michaux C. Fatty acid amide hydrolase: from characterization to therapeutics. Chem. Biodiv. 2007; 4:1882–1902.
3 (a). Kathuria S, Gaetani S, Fegley D, Valino F, Duranti A, Tontini A, Mor M, Tarzia G, La Rana G, Calignano A, Giustino A, Tattoli M, Palmery M, Cuomo V, Piomelli D. Modulation of anxiety

through blockade of anandamide hydrolysis. Nat. Med. 2003; 9:76–81. [PubMed: 12461523] (b) Gobbi G, Bambico FR, Mangieri R, Bortolato M, Campolongo P, Solinas M, Cassano T, Morgese MG, Debonnel G, Duranti A, Tontini A, Tarzia G, Mor M, Trezza V, Goldberg SR, Cuomo V, Piomelli D. Antidepressant-like activity and modulation of brain monoaminergic transmission by blockade of anandamide hydrolysis. Proc. Natl. Acad. Sci USA. 2005; 102:18620–18625. [PubMed: 16352709] (c) Maione S, De Petrocellis L, de Novellis V, Moriello AS, Petrosino S, Palazzo E, Rossi FS, Woodward DF, Di Marzo V. Analgesic actions of N-arachidonoyl-serotonin, a fatty acid amide hydrolase inhibitor with antagonistic activity at vanilloid TRPV1 receptors. Br. J. Pharmacol. 2007; 150:766–781. [PubMed: 17279090] (d) Clapper JR, Moreno-Sanz G, Russo R, Guijarro A, Vacondio F, Duranti A, Tontini A, Sanchini S, Sciolino NR, Spradley JM, Hohmann AG, Calignano A, Mor M, Tarzia G, Piomelli D. Anandamide suppresses pain initiation through a peripheral endocannabinoid mechanism. Nat. Neurosci. 2010; 13:1265–1270. [PubMed: 20852626] (e) Ahn K, Smith SE, Liimatta MB, Beidler D, Sadagopan N, Dudley DT, Young T, Wren P, Zhang Y, Swaney S, Van Becelaere K, Blankman JL, Nomura DK, Bhattachar SN, Stiff C, Nomanbhoy TK, Weerapana E, Johnson DS, Cravatt BF. Mechanistic and pharmacological characterization of PF-04457845: a highly potent and selective fatty acid amide hydrolase inhibitor that reduces inflammatory and noninflammatory pain. J. Pharmacol. Exp. Ther. 2011; 338:114–124. [PubMed: 21505060]

4. Piomelli D, Tarzia G, Duranti A, Tontini A, Mor M, Compton TR, Dasse O, Monaghan EP, Parrott JA, Putman D. Pharmacological profile of the selective FAAH inhibitor KDS-4103 (URB597). CNS Drug Rev. 2006; 12:21–38. [PubMed: 16834756]

5 (a). Petrosino S, Di Marzo V. FAAH and MAGL inhibitors: therapeutic opportunities from regulating endocannabinoid levels. Curr. Opin. Investig. Drugs. 2010; 11:51–62.(b) Mor M, Lodola A. Pharmacological tools in endocannabinoid neurobiology. Curr. Top. Behav. Neurosci. 2009; 1:187–110.(c) Vandevoorde S, Lambert DM. Focus on the three key enzymes hydrolysing endocannabinoids as new drug targets. Curr. Pharm. Des. 2005; 11:2647–2468. [PubMed: 16101463] (d) Piomelli D. The endocannabinoid system: a drug discovery perspective. Curr. Opin. Investig. Drugs. 2005; 6:672–679.(e) Cravatt BF, Lichtman AH. Fatty acid amide hydrolase: an emerging therapeutic target in the endocannabinoid system. Curr. Opin. Chem. Biol. 2003; 7:469–475. [PubMed: 12941421]

6. McKinney MK, Cravatt BF. Structure and function of fatty acid amide hydrolase. Annu. Rev. Biochem. 2005; 74:411–432. [PubMed: 15952893]

7 (a). Cravatt BF, Giang DK, Mayfield SP, Boger DL, Lerner RA, Gilula NB. Molecular characterization of an enzyme that degrades neuromodulatory fatty-acid amides. Nature. 1996; 384:83–87. [PubMed: 8900284] (b) Patricelli MP, Cravatt BF. Clarifying the catalytic roles of conserved residues in the amidase signature family. J. Biol. Chem. 2000; 275:19177–19184. [PubMed: 10764768] (c) McKinney MK, Cravatt BF. Evidence for distinct roles in catalysis for residues of the serine-serine-lysine catalytic triad of fatty acid amide hydrolase. J. Biol. Chem. 2003; 278:37393–37399. [PubMed: 12734197]

8 (a). Lodola A, Mor M, Hermann JC, Tarzia G, Piomelli D, Mulholland AJ. QM/MM modelling of oleamide hydrolysis in fatty acid amide hydrolase (FAAH) reveals a new mechanism of nucleophile activation. Chem. Commun. 2005:4399–4401.(b) Tubert-Brohman I, Acevedo O, Jorgensen WL. Elucidation of hydrolysis mechanisms for fatty acid amide hydrolase and its Lys142Ala variant via QM/MM simulations. J. Am. Chem. Soc. 2006; 128:16904–16913. [PubMed: 17177441] (c) Lodola A, Mor M, Sirirak J, Mulholland AJ. Insights into the mechanism and inhibition of fatty acid amide hydrolase from quantum mechanics/molecular mechanics (QM/MM) modelling. Biochem. Soc. Trans. 2009; 37:363–367. [PubMed: 19290863] (d) Lodola A, Sirirak J, Fey N, Rivara S, Mor M, Mulholland AJ. Structural fluctuations in enzyme-catalyzed reactions: Determinants of reactivity in fatty acid amide hydrolase from multivariate statistical analysis of quantum mechanics/molecular mechanics paths. J. Chem. Theory Comput. 2010; 6:2948–2960.(e) Palermo A, Branduardi D, Masetti M, Lodola A, Mor M, Piomelli D, Cavalli A, De Vivo M. Covalent inhibitors of fatty acid amide hydrolase: a rationale for the activity of piperidine and piperazine aryl ureas. J. Med. Chem. 2011; 54:6612–6623. [PubMed: 21830831]

9. Mileni M, Kamtekar S, Wood DC, Benson TE, Cravatt BF, Stevens RC. Crystal structure of fatty acid amide hydrolase bound to the carbamate inhibitor URB597: discovery of a deacylating water

molecule and insight into enzyme inactivation. J. Mol. Biol. 2010; 400:743–754. [PubMed: 20493882]

10 (a). Otrubova K, Ezzili C, Boger DL. The discovery and development of inhibitors of fatty acid amide hydrolase (FAAH). Bioorg. Med. Chem. Lett. 2011; 21:4674–4685. [PubMed: 21764305] (b) Minkkilä A, Saario S, Nevalainen T. Discovery and development of endocannabinoid-hydrolyzing enzyme inhibitors. Curr. Top. Med. Chem. 2010; 10:828–858. [PubMed: 20370710] (c) Seierstad M, Breitenbucher JG. Discovery and development of fatty acid amide hydrolase (FAAH) inhibitors. J. Med. Chem. 2008; 51:7327–7343. [PubMed: 18983142] (d) Vandevoorde S. Overview of the chemical families of fatty acid amide hydrolase and monoacylglycerol lipase inhibitors. Curr. Top. Med. Chem. 2008; 8:247–267. [PubMed: 18289091] (e) Lambert DM, Fowler CJ. The endocannabinoid system: drug targets, lead compounds, and potential therapeutic applications. J. Med. Chem. 2005; 48:5059–5087. [PubMed: 16078824]

11. Mor M, Rivara S, Lodola A, Plazzi PV, Tarzia G, Duranti A, Tontini A, Piersanti G, Kathuria S, Piomelli D. Cyclohexylcarbamic acid 3′- or 4′-substituted biphenyl-3-yl esters as fatty acid amide hydrolase inhibitors: synthesis, quantitative structure-activity relationships, and molecular modeling studies. J. Med. Chem. 2004; 47:4998–5008. [PubMed: 15456244]

12. Lodola A, Rivara S, Mor M. Application of computational methods to the design of fatty acid amide hydrolase (FAAH) inhibitors based on a carbamic template structure. Adv. Protein. Chem. Struct. Biol. 2011; 85:1–26. [PubMed: 21920320]

13. Alexander JP, Cravatt BF. Mechanism of carbamate inactivation of FAAH: implications for the design of covalent inhibitors and in vivo functional probes for enzymes. Chem. Biol. 2005; 12:1179–1187. [PubMed: 16298297]

14. Lodola A, Mor M, Rivara S, Christov C, Tarzia G, Piomelli D, Mulholland AJ. Identification of productive inhibitor binding orientation in fatty acid amide hydrolase (FAAH) by QM/MM mechanistic modelling. Chem. Commun. 2008:214–216.

15. Lodola A, Capoferri L, Rivara S, Chudyk E, Sirirak J, Dyguda-Kazimierowicz E, Sokalski WA, Mileni M, Tarzia G, Piomelli D, Mor M, Mulholland AJ. Understanding the role of carbamate reactivity in fatty acid amide hydrolase inhibition by QM/MM mechanistic modelling. Chem. Commun. 2011; 47:214–216.

16. Mileni M, Johnson DS, Wang Z, Everdeen DS, Liimatta M, Pabst B, Bhattacharya K, Nugent RA, Kamtekar S, Cravatt BF, Ahn K, Stevens RC. Structure-guided inhibitor design for human FAAH by interspecies active site conversion. Proc. Natl. Acad. Sci. USA. 2008; 105:12820–12824. [PubMed: 18753625]

17. Keith JM, Apodaca R, Xiao W, Seierstad M, Pattabiraman K, Wu J, Webb M, Karbarz MJ, Brown S, Wilson S, Scott B, Tham CS, Luo L, Palmer J, Wennerholm M, Chaplan S, Breitenbucher JG. Thiadiazolopiperazinyl ureas as inhibitors of fatty acid amide hydrolase. Bioorg. Med. Chem. Lett. 2008; 18:4838–4843. [PubMed: 18693015]

18. Ahn K, Johnson DS, Fitzgerald LR, Liimatta M, Arendse A, Stevenson T, Lund ET, Nugent RA, Nomanbhoy TK, Alexander JP, Cravatt BF. Novel mechanistic class of fatty acid amide hydrolase inhibitors with remarkable selectivity. Biochemistry. 2007; 46:13019–13030. [PubMed: 17949010]

19. Sykes NO, Macdonald SJ, Page MI. Acylating agents as enzyme inhibitors and understanding their reactivity for drug design. J. Med. Chem. 2002; 45:2850–2856. [PubMed: 12061887]

20. Karbarz MJ, Luo L, Chang L, Tham CS, Palmer JA, Wilson SJ, Wennerholm ML, Brown SM, Scott BP, Apodaca RL, Keith JM, Wu J, Breitenbucher JG, Chaplan SR, Webb M. Biochemical and biological properties of 4-(3-phenyl-[1,2,4] thiadiazol-5-yl)-piperazine-1-carboxylic acid phenylamide, a mechanism-based inhibitor of fatty acid amide hydrolase. Anesth. Analg. 2009; 108:316–329. [PubMed: 19095868]

21. Butini S, Brindisi M, Gemma S, Minetti P, Cabri W, Gallo G, Vincenti S, Talamonti E, Borsini F, Caprioli A, Stasi MA, di Serio S, Ros S, Borrelli G, Maramai S, Fezza F, Campiani G, Maccarrone M. Discovery of Potent Inhibitors of Human and Mouse Fatty Acid Amide Hydrolases. J. Med. Chem. 2012; 55:6898–6915. [PubMed: 22779702]

22 (a). Warshel A, Levitt M. Theoretical studies of enzymic reactions: dielectric, electrostatic and steric stabilization of the carbonium ion in the reaction of lysozyme. J. Mol. Biol. 1976; 103:227–249. [PubMed: 985660] (b) Field MJ, Bash PA, Karplus M. A combined quantum

mechanical and molecular mechanical potential for molecular dynamics simulations. J. Comput. Chem. 1990; 11:700–733.(c) Gao, J. Methods and applications of combined quantum mechanical and molecular mechanical potentials. In: Lipkowitz, KB.; Boyd, DR., editors. Reviews in Computational Chemistry. Vol. Vol. 7. VCH Publishers; New York: 1996. p. 119-185.(d) Warshel A. Computer simulations of enzyme catalysis: methods, progress, and insights. Annu. Rev. Biophys. Biomol. Struct. 2005; 32:425–443. [PubMed: 12574064]

23 (a). Lonsdale R, Ranaghan KE, Mulholland AJ. Computational enzymology. Chem. Commun. 2010; 46:2354–2372.(b) Senn HM, Thiel W. QM/MM methods for biomolecular systems. Angew. Chem. Int. Ed. Engl. 2009; 48:1198–1229. [PubMed: 19173328] (c) van der Kamp MW, Mulholland AJ. Computational enzymology: insight into biological catalysts from modelling. Nat. Prod. Rep. 2008; 25:1001–1014. [PubMed: 19030602] (d) Cavalli A, Carloni P, Recanatini M. Target-related applications of first principles quantum chemical methods in drug design. Chem. Rev. 2006; 106:3497–3519. [PubMed: 16967914]

24 (a). Lodola A, De Vivo M. The Increasing Role of QM/MM in Drug Discovery. Adv. Protein Chem. Struct. Biol. 2012; 87:337–362. [PubMed: 22607760] (b) De Vivo M. Bridging quantum mechanics and structure-based drug design. Front. Biosci. 2011; 1:1619–1633. [PubMed: 21196252] (c) Mulholland AJ. Modelling enzyme reaction mechanisms, specificity and catalysis. Drug Discov. Today. 2005; 10:1393–1402. [PubMed: 16253878]

25. Elstner M. The SCC-DFTB method and its application to biological systems. Theor. Chem. Acc. 2006; 116:316–325.

26. MacKerell AD, Bashford D, Bellott M, Dunbrack RL, Evanseck JD, Field MJ, Fischer S, Gao J, Guo H, Ha S, Joseph-McCarthy D, Kuchnir L, Kuczera K, Lau FTK, Mattos C, Michnick S, Ngo T, Nguyen DT, Prodhom B, Reiher WE, Roux B, Schlenkrich M, Smith JC, Stote R, Straub J, Watanabe M, Wiorkiewicz-Kuczera J, Yin D, Karplus M. All-Atom Empirical Potential for Molecular Modeling and Dynamics Studies of Proteins. J. Phys. Chem. A. 1998; 102:3586–3616.

27. Lonsdale R, Harvey JN, Mulholland AJ. A practical guide to modelling enzyme-catalysed reactions. Chem. Soc. Rev. 2012; 41:3025–3038. [PubMed: 22278388]

28. Patricelli MP, Lovato MA, Cravatt BF. Chemical and mutagenic investigations of fatty acid amide hydrolase: evidence for a family of serine hydrolases with distinct catalytic properties. Biochemistry. 1999; 38:9804–9812. [PubMed: 10433686]

29. Brooks BR, Brooks CL 3rd, Mackerell AD, Nilsson L, Petrella RJ, Roux B, Won Y, Archontis G, Bartels C, Boresch S, Caflisch A, Caves L, Cui Q, Dinner AR, Feig M, Fischer S, Gao J, Hodoscek M, Im W, Kuczera K, Lazaridis T, Ma J, Ovchinnikov V, Paci E, Pastor RW, Post CB, Pu JZ, Schaefer M, Tidor B, Venable RM, Woodcock HL, Wu X, Yang W, York DM, Karplus M. CHARMM: the biomolecular simulation program. J. Comput. Chem. 2009; 30:1545–1614. www.charmm.org. [PubMed: 19444816]

30. Cui Q, Elstner M, Kaxiras E, Frauenheim T, Karplus M. A QM/MM Implementation of the Self-Consistent Charge Density Functional Tight Binding (SCC-DFTB) Method. J. Phys. Chem. B. 2001; 105:569–585.

31 (a). Woodcock H,L, Hodoscek M, Brooks BR. Exploring SCC-DFTB paths for mapping QM/MM reaction mechanisms. J. Phys. Chem. A. 2007; 111:5720–5728. [PubMed: 17555303] (b) Riccardi D, Schaefer P, Yang Y, Yu H, Ghosh N, Prat-Resina X, König P, Li G, Xu D, Guo H, Elstner M, Cui Q. Development of effective quantum mechanical/molecular mechanical (QM/MM) methods for complex biological processes. J. Phys. Chem. B. 2006; 110:6458–6469. [PubMed: 16570942] (c) Xu D, Guo H, Cui Q. Antibiotic deactivation by a dizinc beta-lactamase: mechanistic insights from QM/MM and DFT studies. J. Am. Chem. Soc. 2007; 129:10814–10822. [PubMed: 17691780] (d) Barnett CB, Wilkinson KA, Naidoo KJ. Molecular details from computational reaction dynamics for the cellobiohydrolase I glycosylation reaction. J. Am. Chem. Soc. 2011; 133:19474–19482. [PubMed: 22007863] (e) Mujika JI, Lopez X, Mulholland AJ. Mechanism of C-terminal intein cleavage in protein splicing from QM/MM molecular dynamics simulations. Org. Biomol. Chem. 2012; 10:1207–1218. [PubMed: 22179261] (f) Lodola A, Branduardi D, Capoferri L, De Vivo M, Mor M, Piomelli D. A catalytic mechanism for cysteine N-terminal nucleophile hydrolases, as revealed by free energy simulations. Plos One. 2012; 7:e32397. [PubMed: 22389698]

32. Capoferri L, Mor M, Sirirak J, Chudyk E, Mulholland AJ, Lodola A. Application of a SCC-DFTB QM/MM approach to the investigation of the catalytic mechanism of fatty acid amide hydrolase. J. Mol. Model. 2011; 17:2375–2383. [PubMed: 21365225]

33. Jorgensen WL, Chandrasekhar J, Madura JD, Impey RW, Klein ML. Comparison of Simple Potential Functions for Simulating Liquid Water. J. Chem. Phys. 1983; 79:926–935.

34. Brooks CL III, Karplus M. Deformable stochastic boundaries in molecular dynamics. J. Chem. Phys. 1983; 79:6312–6325.

35. Ridder L, Harvey JN, Rietjens IMCM, Vervoort J, Mulholland AJ. Ab Initio QM/MM Modeling of the Hydroxylation Step in p-Hydroxybenzoate Hydroxylase. J. Phys. Chem. B. 2003; 107:2118–2126.

36. Hermann JC, Hensen C, Ridder L, Mulholland AJ, Holtje HD. Mechanisms of Antibiotic Resistance: QM/MM Modeling of the Acylation Reaction of a Class A β-Lactamase with Benzylpenicillin. J. Am. Chem. Soc. 2005; 127:4454–4465. [PubMed: 15783228]

37. Jaguar. version 7.8. Schrödinger, LLC; New York, NY: 2011.

38. Claeyssens F, Ranaghan KE, Lawan N, Macrae SJ, Manby FR, Harvey JN, Mulholland AJ. Analysis of chorismate mutase catalysis by QM/MM modelling of enzyme-catalysed and uncatalysed reactions. Org. Biomol. Chem. 2011; 9:1578–1590. [PubMed: 21243152]

39. Mulholland AJ, Richards G. Acetyl-CoA enolization in citrate synthase: a quantum mechanical/molecular mechanical (QM/MM) study. Proteins. 1997; 27:9–25. [PubMed: 9037708]

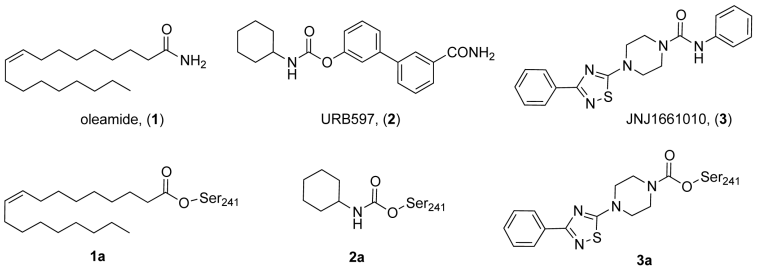

Figure 1.

FAAH substrate (**1**), and inhibitors (**2**, **3**) considered in this study and representation of the corresponding covalent adducts (**1a**, **2a**, **3a**) with Ser241.

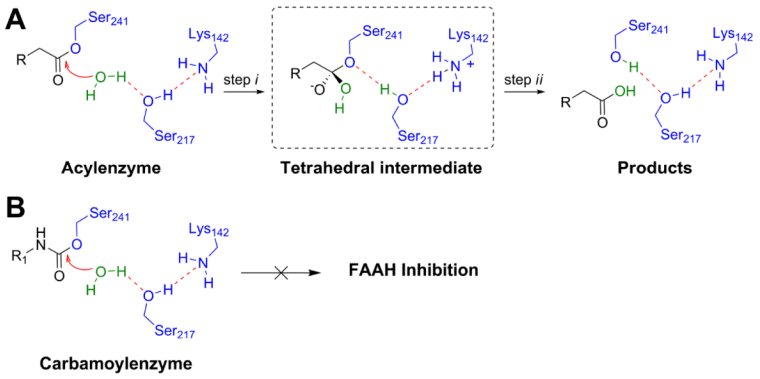

Figure 2.

(A) Mechanism of hydrolysis of acylated FAAH.[9] (B) When the nucleophile serine is carbamoylated (as in the case of URB597) the reaction does not occur in a short time-scale. The water molecule depicted in green corresponds to the deacylating water molecule W1.

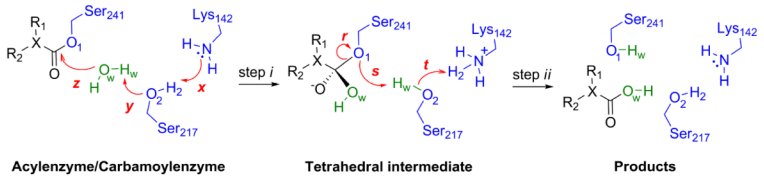

Figure 3.

Individual reaction processes (***x***, ***y***, ***z***, ***r***, ***s***, ***t***) involved in the deacylation or decarbamoylation of FAAH. General formulas of catalytic residues with the adduct product of Ser241 and oleamide, X = C; R_1=H; R_2 = (Z)-octadec-9-enyl; URB597, X = N; R_1= H; R_2 = cyclohexyl; compound **3**, R_1, R_2, X = 4-(3-phenyl-1,2,4-thiadiazol-5-yl)piperazin-1-yl.

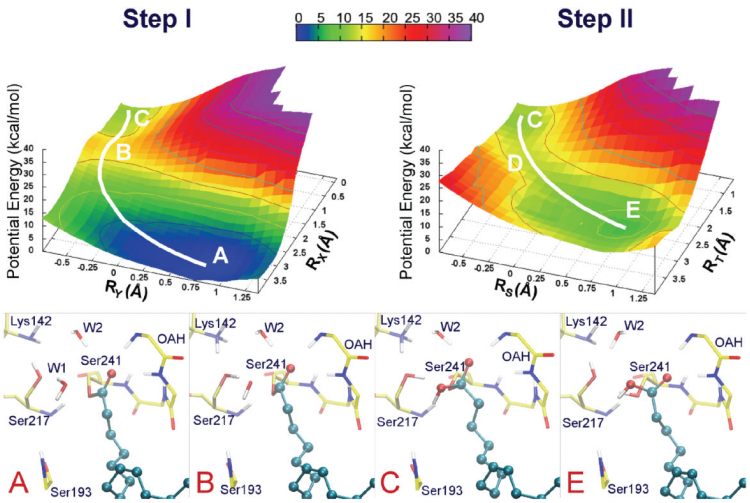

Figure 4.

SCC-DFTB/CHARMM27 QM/MM PESs (top) for deacylation of adduct **1a**. The structures of some configurations are also shown (bottom): **A** (acylenzyme), **B** (transition state 1), **C** (tetrahedral intermediate), **E** (free enzyme and oleic acid). FAAH active site residues are represented by yellow carbon atoms, while the carbon atoms of the (Z)-octadec-9-enyl fragment of oleamide are depicted in cyan.

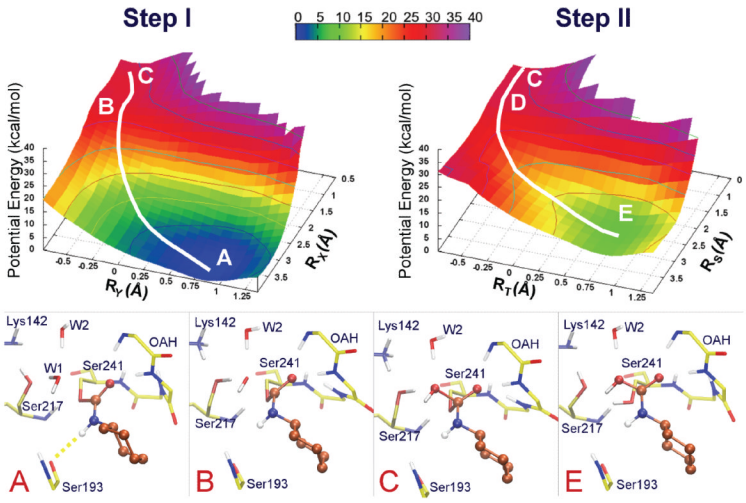

Figure 5.

SCC-DFTB/CHARMM27 QM/MM PESs (top) for decarbamoylation of adduct **2a**. The structures of some configurations (bottom) are also shown: **A** (carbamoylenzyme), **B** (transition state 1), **C** (tetrahedral intermediate), **E** (free enzyme and cyclohexylcarbamic acid). FAAH active-site residues are represented by yellow carbon atoms, while the carbon atoms of the carbamoylating fragment of URB597 are depicted in orange.

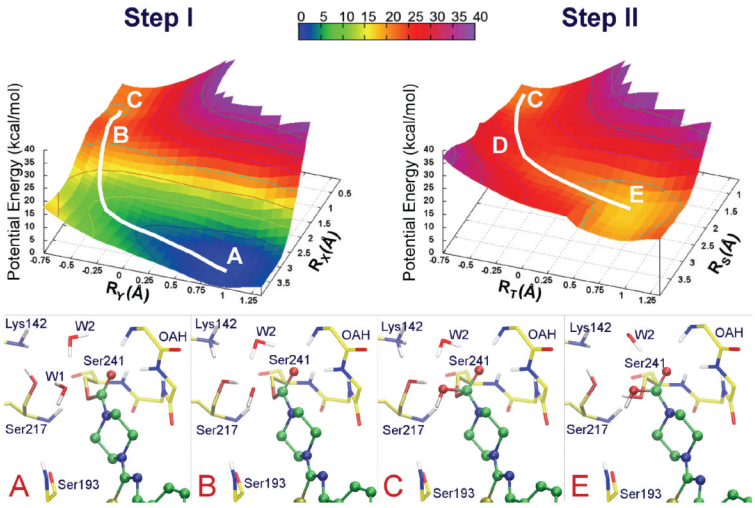

Figure 6.

SCC-DFTB/CHARMM27 QM/MM PESs (top) for decarbamoylation of adduct **3a**. The structures of some configurations (bottom) are also shown: **A** (carbamoylenzyme), **B** (transition state 1), **C** (tetrahedral intermediate), **E** (free enzyme and 4-(3-phenyl-1,2,4-thiadiazol-5-yl)piperazin-1-yl carbamic acid). FAAH active site residues are represented by yellow carbon atoms, while the carbon atoms of the carbamoylating fragment of **3** are depicted in green.

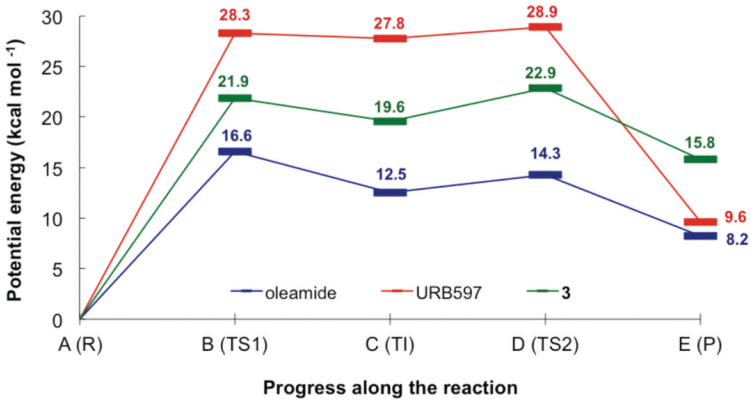

Figure 7.

SCC-DFTB/CHARMM27 potential energy profiles for deacylation/decarbamoylation of the covalent adducts involving oleamide (blue), URB597 (red) and *N*-piperazinylurea **3** (green). The relevant configurations are: acyl/carbamoylenzyme (**A**), TS1 (**B**), TI (**C**), TS2 (**D**), free enzyme and acid (**E)**. R stands for reactants, P for products.

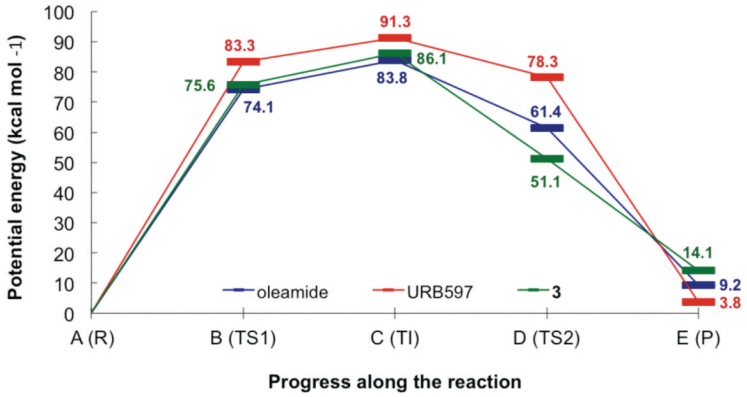

Figure 8.

Gas-phase SCC-DFTB potential energy profile of the QM region. Reported values are obtained from single-point calculations on the QM regions of the relevant configurations for deacylation/decarbamoylation of the covalent adducts involving oleamide (blue), URB597 (red) and *N*-piperazinylurea **3** (green). Reported configurations are: acyl/carbamoylenzyme (**A**), TS1 (**B**), TI (**C**), TS2 (**D**), free enzyme and acid (**E**). R stands for reactants, P for products.

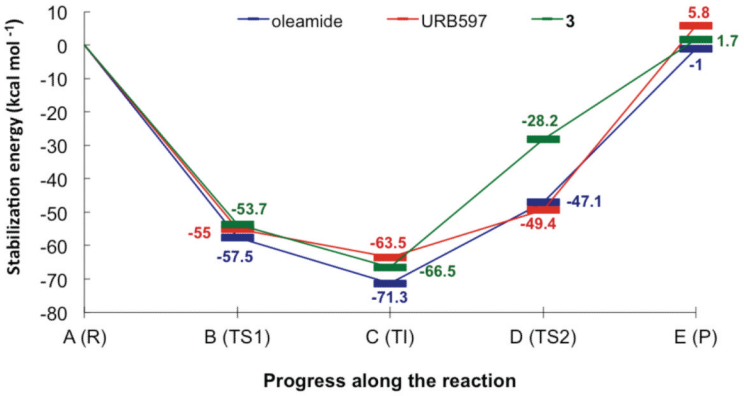

Figure 9.

Stabilization energy along the deacylation/decarbamoylation path of the covalent adducts involving oleamide (blue), URB597 (red) and *N*-piperazinylurea **3** (green). Reported configurations are: acyl/carbamoylenzyme (**A**); TS1 (**B**); TI (**C**); TS2 (**D**); free enzyme and acid (**E**). R stands for reactants, P for products.

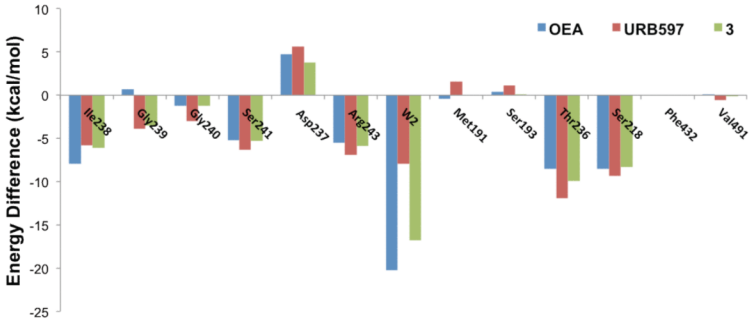

Figure 10.

Decomposition analysis. The QM/MM stabilization energy contributions of MM residues on the TI (state **C**), for covalent adducts **1**-**3**, involving oleamide (blue), URB597 (red) and *N*-piperazinylurea **3** (green), respectively. Negative values correspond to stabilization, positive ones to destabilization. Energies are relative to configuration **A** of each system.

Table 1

Distances in Å between atoms involved in the formation or in the breakage of covalent bonds for relevant configuration identified during the deacylation of FAAH starting from adduct 1a. Atom labels are consistent with Figure 3.

	O_w-C	O_w- H_w	O_2-H_w	O_2-H_2	N-H_2	O_1-C	O_1-H_w	O-C
Acylenzime (**A**)	2.48	0.99	1.78	1.01	1.88	1.36	2.53	1.24
TS1 (**B**)	1.84	1.38	1.11	1.69	1.06	1.44	2.45	1.29
TI (**C**)	1.47	1.66	1.02	1.69	1.06	1.614	2.49	1.34
TS2 (**D**)	1.41	2.65	1.15	1.53	1.11	1.91	1.29	1.28
Products (**E**)	1.40	2.45	1.80	1.03	1.80	2.17	0.99	1.23

Table 2

Distances in Å between atoms involved in the formation or in the breakage of covalent bonds for relevant configurations identified during the decarbamoylation of FAAH starting from adduct 2a.

	O_w-C	O_w- H_w	O_2-H_w	O_2-H_2	N-H_2	O_1-C	O_1-H_w	O-C
Carbamoylenzyme (**A**)	2.66	0.99	1.80	1.01	1.88	1.37	2.46	1.25
TS1 (**B**)	1.82	1.44	1.09	1.69	1.06	1.46	2.50	1.29
TI (**C**)	1.57	1.80	1.01	1.69	1.06	1.54	2.40	1.32
TS2 (**D**)	1.47	2.39	1.07	1.70	1.07	1.79	1.50	1.29
Products (**E**)	1.39	2.44	1.88	1.01	1.88	2.26	0.99	1.25

Table 3

Distances in Å between atoms involved in the formation or in the breakage of covalent bonds for relevant configuration identified during the decarbamoylation of FAAH starting from adduct 3a.

	O_w-C	O_w- H_w	O_2-H_w	O_2-H_2	N-H_2	O_1-C	O_1-H_w	O-C
Carbamoylenzyme (**A**)	2.49	0.98	1.82	0.99	2.01	1.37	2.46	1.24
TS1 (**B**)	1.83	1.40	1.10	1.73	1.06	1.44	2.43	1.29
TI (**C**)	1.53	1.80	1.00	1.74	1.06	1.53	2.32	1.32
TS2 (**D**)	1.38	2.40	1.55	1.36	1.18	2.11	1.04	1.24
Products (**E**)	1.40	2.31	1.69	1.00	1.92	2.14	1.01	1.23

Table 4

SCC-DFTB/CHARMM27 energy values (kcal mol^{-1}, mean value ± standard error of the mean) for key configurations (B, C, D and E) obtained from deacylation/decarbamoylation of the covalent adducts 1a (oleamide), 2a (URB597) and 3a (*N*-piperazinylurea 3).

	TS1 (B)[a]	**TI (C)**[a]	**TS2 (D)**[a]	**Products (E)**[a]
Adduct **1a** (oleamide)	19.1 ± 0.5	16.6 ± 0.9	17.6 ± 0.7	8.9 ± 0.5
Adduct **2a** (URB597)	31.7 ± 0.9	31.1 ± 0.8	31.0 ± 0.6	10.6 ± 0.6
Adduct **3a** (N-piperazinylurea **3**)	22.9 ± 0.8	22.3 ± 1.0	25.8 ± 0.7	17.6 ± 0.6

[a]Mean values and SEMs were calculated from SCC-DFTB/CHARM27 energy, obtained from seven additional simulations.

Table 5

SCC-DFTB/CHARMM27 and B3LYP/6-31+G(d)//SCC-DFTB/CHARMM27 potential energy values (expressed in kcal mol^{-1}) for key configurations (B, C, D and E) obtained from deacylation/decarbamoylation of the covalent adducts 1a (oleamide), 2a (URB597) and 3a (*N*-piperazinylurea 3).

	Adduct 1a		Adduct 2a		Adduct 3a	
	SCC-DFTB[a]	B3LYP[b]	SCC-DFTB[a]	B3LYP[b]	SCC-DFTB[a]	B3LYP[b]
TS1 (**B**)	16.6	17.4	28.3	28.0	21.9	20.0
TI (**C**)	12.5	16.4	27.8	27.8	19.6	19.2
TS2 (**D**)	14.3	(15.9)[c]	28.9	28.9	22.9	21.0
Products (**E**)	8.2	11.1	9.6	15.5	15.8	10.3

[a]Performed at SCC-DFTB/CHARMM27 level

[b]Performed at B3LYP/6-31+G(d)//SCC-DFTB/CHARMM27 level

[c]**D** is no longer a stationary point on B3LYP/6-31G+(d)//SCC-DFTB/CHARMM27 surface